Molecular Motors Enhance Microtubule Lattice Plasticity

William Lecompte and Karin John ⓘ*
Université Grenoble Alpes, CNRS, LIPhy, 38000 Grenoble, France

Microtubules are key structural elements of living cells that are crucial for cell division, intracellular transport, and motility. Recent experiments have shown that microtubule-severing proteins and molecular motors stimulate the direct and localized incorporation of free tubulin into the shaft. However, a mechanistic picture of how microtubule-associated proteins affect the lattice is completely missing. Here we theoretically explore a potential mechanism of lattice turnover stimulated by processive molecular motors in which a weak transient destabilization of the lattice by the motor stepping promotes the formation of mobile vacancies. In the absence of free tubulin the defect rapidly propagates, leading to a complete fracture. In the presence of free tubulin, the motor walk induces a vacancy drift in the direction opposite of the motor walk. The drift is accompanied by the direct and localized incorporation of free tubulin along the trajectory of the vacancy. Our results are consistent with experiments and strongly suggest that a weak lattice-motor interaction is responsible for an augmented microtubule shaft plasticity.

I. INTRODUCTION

Microtubules (MTs) are self-organized polar tubelike polymers and constitute a major component of the cytoskeleton. They play a central role in cell division, intracellular transport, and motility. MTs are dynamic dissipative structures, which grow or shrink primarily by tubulin dimer addition or removal at their extremities, labeled $(+)$ and $(-)$ ends. Their nonequilibrium behavior results from the irreversible hydrolysis of GTP tubulin into GDP tubulin upon polymerization [1] and manifests itself as stochastic transitions between growth and shrinkage phases, called dynamic instability [2–6]. The dynamic instability of the MT tip has been a major focus of MT research over the past 30 years. In contrast, the MT shaft has been considered as an inert structure, due to the high stability of the intact lattice far away from the extremities [7]. However, an early experiment with end-stabilized MTs by Dye *et al.* [8] clearly showed that the shaft may lose and incorporate tubulin dimers directly. Later it was shown that GTP dimers (or dimers in the GTP conformation) exist outside of the cap region [9], without a clear picture of how the GTP state could survive sufficiently long to be detectable in the shaft. A very recent series of experiments revealed that the shaft lattice exhibits a spontaneous dynamics, part of which is linked to lattice dislocations [10,11]. Perturbing the lattice externally via periodic weak mechanical forcing [12] or the activity of MT-associated proteins, e.g., MT-severing enzymes or molecular motors [13–16], has been shown to

facilitate the localized incorporation of tubulin dimers from the surrounding medium into the lattice. Furthermore, regions of high curvature or regions in close contact either with a surface or another microtubule could be sites of direct tubulin exchange [17].

It has been shown experimentally and theoretically that dislocations are preferential sites of lattice dynamics [11]. These structures are inherent in the lattice and are created during the polymerization process. The same holds for recently identified multiseam MTs [18], which entail the existence of point defects of the size of a tubulin monomer. However, the experimentally observed increase in shaft plasticity due to severing enzymes and molecular motors [13–16] suggests the nucleation of defects in the intact lattice. One obvious possibility of *de novo* created sites of lattice exchange are vacancies of the size of a single tubulin dimer. These point defects have been identified by scanning force microscopy of dynamic MTs [19] and it has already been speculated that long-lived point defects may serve as a point of attack for MT-severing enzymes [20]. A recent experiment suggests that the combined walk of several kinesins is able remove tubulin dimers from the lattice [21].

Here, we explore theoretically the role of point defects in the MT shaft plasticity in the presence of molecular motors. Thereby we employ the term "plasticity" to denote the removal of tubulin dimers from the MT lattice or the integration of tubulin dimers into the MT lattice far away from the MT extremities. Our objective is to provide a first mechanistic concept consistent with recent experiments on MT-motor interactions [14–16]. To that end we employ a kinetic Monte Carlo model and investigate (i) the kinetics of the formation of point defects, (ii) the progression of the defect size until complete MT fracture in the absence of free tubulin, and (iii) the dynamics of point defects in the presence of free tubulin. These processes will be studied in the absence and presence of processive molecular motors, which transiently and locally

---
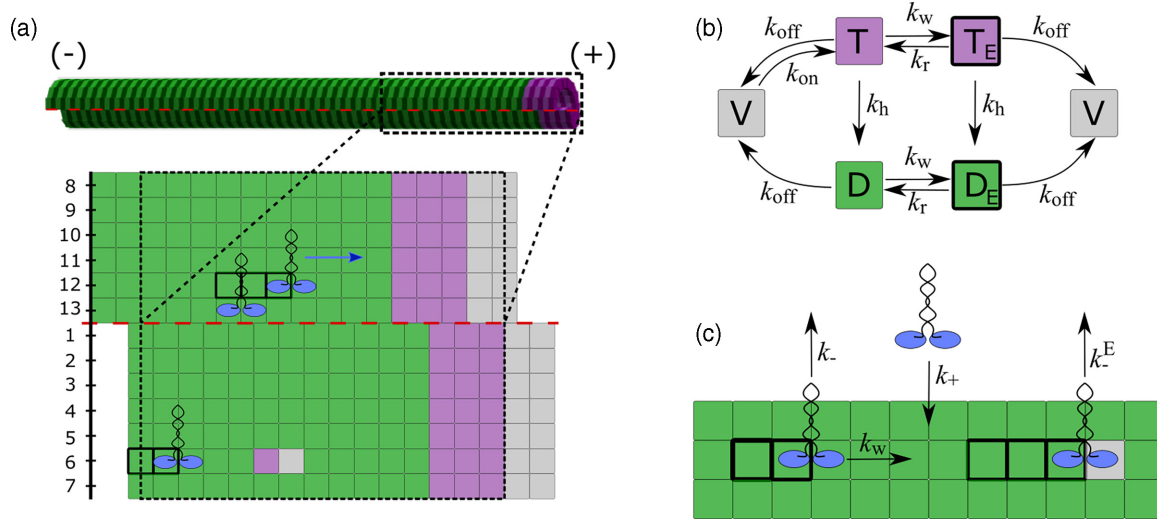
*karin.john@univ-grenoble-alpes.fr

FIG. 1. Schematic setup of the kinetic Monte Carlo model for the MT lattice and processive (+)-end directed molecular motors. (a) The canonical lattice configuration with (+)-end directed processive motors. Vacant lattice sites are gray, GTP dimers are pink, and GDP dimers are green. Dimers with strong contours are in the excited state as explained in the text. (b) Summary of the kinetic transitions of lattice dimers. T (D) denotes GTP (GDP) dimers and V denotes vacant lattice sites. The subscript E denotes the excited state. The color code is as in (a). (c) Summary of the kinetic transitions for molecular motors.

weakly destabilize the lattice as they walk along the lattice. Since many details of the dynamic properties of the MT shaft lattice are unknown, we are focusing on very basic processes to recover the relevant length and time-scale of the MT shaft dynamics that were observed experimentally.

II. MODEL

We use a simple and robust kinetic Monte Carlo model to investigate the MT shaft dynamics in the presence of processive molecular motors. The basic model setup and kinetic transitions are schematically summarized in Fig. 1. Similar types of kinetic Monte Carlo models have been used, e.g., to study the microtubule tip dynamics [22–26], the dynamics of dislocations in the MT shaft [11], and the dynamics of motors walking along the lattice [27]. The model parameters (see Table I) are comparable to values found in the literature and are adapted to reproduce typical polymerization ($\sim$2 µm min^{-1}) and depolymerization speeds ($\sim$20 µm min^{-1}) of the MT tip, the dynamic instability of the MT (+) end (cf. Fig. 5), and the typical motor speeds and run length for kinesin and yeast dynein motors. Here, we specifically aim to study the creation and dynamics of dimer vacancies in the presence of motors using a basic set of kinetic transitions previously established and amended by weak motor-lattice interactions

a. MT lattice structure. We model the canonical microtubule lattice (13 protofilaments, three-start left-handed helix [28,29]) as a square lattice on the scale of the dimer; i.e., each dimer has two longitudinal and two lateral neighbors as previously introduced [11,22,24]. The lattice is periodic in a direction perpendicular to the long axis of the microtubule with an offset of 3/2 lattice sites to reproduce the seam structure [see Fig. 1(a)]. Lattice sites can be either empty or occupied by GTP-bound (T) or GDP-bound (D) dimers. Dimers interact with other dimers on nearest-neighbor lattice

sites via attractive interactions, characterized by bond energies ΔG_1 and ΔG_2 for longitudinal and lateral bonds, respectively. Each dimer-dimer contact across the seam is counted with a binding energy $\Delta G_2/2$; i.e., in the fully occupied lattice, dimers at the seam have the same binding energy as dimers in the bulk lattice. We assume that longitudinal bonds of T-T contacts are further stabilized by the energy, ΔG_1^T [30–32]. We assume a lattice anisotropy in the binding energies of $\Delta G_1/\Delta G_2 = 2$, that is, longitudinal contacts are twice as stable as lateral contacts in the GDP lattice, consistent with estimates obtained by kinetic modeling of the MT tip dynamics [22] and molecular dynamics simulations [33].

b. Basic MT lattice transitions. We consider the following transitions: free GTP dimers can polymerize into a lattice structure, bound GTP dimers can depolymerize from the lattice or hydrolyze into GDP dimers, and bound GDP dimers can depolymerize from the lattice [Fig. 1(b)]. GTP dimers attach to a vacant lattice site with rate constant k_{on}, if at least one neighboring lattice site is occupied by a dimer. We assume an infinite reservoir of free GTP-tubulin dimers at concentration c. We do not consider the attachment of GDP dimers; i.e., for free tubulin the exchange GDP $\rightarrow$ GTP is rapid compared to dimer attachment. Dimers detach from the lattice with rate constant k_{off} depending on their lattice environment (for details see the Appendix):

$$k_{off} = k_{off}^* e^{\beta(\Delta G_b + \delta - \Delta G^*)}, \qquad (1)$$

where $\beta^{-1} = k_B T$ is the thermal energy, ΔG_b denotes the binding energy (upon transferring a free dimer from the solution into the lattice), δ denotes a (weak, transient) contribution due to lattice-motor interactions, and ΔG^* denotes the binding energy at the microtubule tip with a GTP cap (i.e., the binding energy of a GTP dimer with one lateral and one longitudinal GTP-dimer neighbor). k_{off}^* denotes the reference off-rate constant for a dimer with binding energy $\Delta G_b = \Delta G^*$ (see

Table I). It defines the timescale $\tau = (k_{\text{off}}^*)^{-1} \approx 1$ s, which has been obtained by calibrating the tip dynamics with experimentally measured velocities of MT growth and shrinkage.

GTP dimers are irreversibly hydrolyzed into GDP dimers by the rate constant k_{h} if their hydrolyzable β subunit is in contact with the α subunit of another dimer, that is, if the longitudinal lattice site in the direction of the microtubule (+) end is occupied [34].

One key assumption, relevant only for the MT shaft, is a steric hindrance for GTP dimers to integrate or leave the GDP lattice, if all four neighboring lattice sites are occupied by dimers and if the two lateral neighbors are GDP dimers. Here we follow the observationthat the more extended (in the direction of the protofilament) conformation of GTP dimers compared to GDP dimers [30,35] prevents the integration or removal of a GTP dimer in a GDP-lattice environment, comparable to stacked LEGO bricks. This mechanism has no consequences for the dynamics of the microtubule tip; however, it has far-reaching consequences for the microtubule shaft: once a GDP dimer has left its GDP-lattice environment and created a point defect, this point defect cannot be closed immediately by integrating a free GTP-tubulin dimer from the solution. We will investigate the consequences of this effect extensively in the Results section.

c. Transitions of molecular motors. The driven transport of molecular motors along protofilaments has been studied in detail before (see, e.g., the review in Ref. [36]). Here, we used a motor dynamics described by a totally asymmetric simple exclusion process (TASEP) supplemented by attachment and detachment processes as studied, e.g., in Refs. [27,37]. The relevant kinetic transitions for motors are summarized in Fig. 1(c). Here we consider two types of motors, fast kinesinlike (+)-end directed motors [38,39] and more slow yeast-dynein-like (−)-end directed motors [40–42]. Molecular motors can bind to two adjacent unoccupied tubulin dimers along the same protofilament with rate constant k_+ and may detach from the microtubule, when bound to two dimers, with rate constant k_- or, when bound to one dimer, with rate constant $k_-^{\text{E}} = \theta k_-$ [43]. Here we assume a fast motor detachment with $\theta = 100$. Lattice bound motors step along the microtubule in a single direction (i.e., kinesin towards the (+) end, dyneins towards the (−) end) with rate constant k_w, if the next lattice site in the stepping direction in not occupied by another motor. We only allow motors to step forward if their front head (in the walking direction) is bound to a dimer. If a motor is bound to the lattice by a single dimer (i.e., the second head occupies a vacancy) the underlying dimer may detach from the lattice (with k_{off}), taking thereby the motor with it.

d. Motor-lattice interactions. We consider two types of lattice-motor interactions:

(i) Two tubulin dimers which are bound to the same motor are not authorized to leave the lattice.

(ii) The irreversible motor step along the protofilament transiently "excites" the underlying tubulin lattice, inducing a slightly less stable ("excited") conformation; i.e., tubulin dimers (situated under the front head of a bound motor) are excited by the motor walk with rate constant k_{w} by the weak energy increment δ [see Eq. (1)] and relax back to the "ground" state with the rate constant k_{r}. The excitation

reaction represents the crucial coupling mechanism between the motor walk and the underlying MT lattice.

A characterization of the steady-state behavior of motors (density, flux) and the fractions of excited and ground-state dimers, ϕ_e and ϕ_g, depending on the ratio of motor attachment and detachment rate constants $\mu = k_+/k_-$ and the ratio of motor stepping rate constant and lattice relaxation rate constant $\nu = k_{\text{w}}/k_{\text{r}}$ can be found in Fig. 6.

III. RESULTS

In the following we will fix the majority of the parameters (see Table I) and analyze the MT lattice depending on the motor density on the MT and the lattice excitation δ. We will focus on "fast" kinesin motors and present some additional results for "slow" dyneins.

A. Creation of point defects

When a motor walks along a perfect lattice (i.e., no point defect present along the protofilament), at each step an underlying tubulin dimer is weakly destabilized by the energy penalty δ. In the following we will explore this effect on the initial creation of a point defect (a single missing dimer or vacancy) and, vice versa, the effect of the existence of a point defect on the motor walk and the consequence for the lattice stability in the vicinity of the defect.

Figure 2(a) shows the fraction of excited and ground-state dimers which can potentially leave the lattice (i.e., they are not sterically blocked by a bound motor) for fast motors (kinesins) depending on the steady-state density of motors on the lattice. The fractions can be roughly estimated using the mean-field approach by [27]

$$\phi_{\text{e}} = (1 - 2\rho)\frac{J}{J + k_{\text{r}}}, \tag{2}$$

$$\phi_{\text{g}} = (1 - 2\rho)\frac{k_r}{J + k_{\text{r}}}, \tag{3}$$

where ρ denotes the steady-state density of motor front heads and

$$J = k_{\text{w}}\rho\frac{1 - 2\rho}{1 - \rho} \tag{4}$$

denotes the steady-state motor flux. The mean-field estimates [dashed lines in Fig. 2(a)] are slightly off the numerical results which is probably a consequence of the localized appearance of excited dimers and the strong correlations with the motor positions. For low motor densities the fraction of "excited" dimers is increasing at the expense of the fraction of "ground-state" dimers. However, for high motor densities, both fractions of excited and ground-state dimers are decreasing. The behavior reflects the jamming of motors (which reduces excitation of dimers) and the blocking of dimers from leaving the lattice by the bound motors.

If motors encounter a point defect, the steady-state motor density is perturbed since motors cannot walk "over" the point defect and have to detach [see Fig. 2(b)]. For fast motor detachment at the defect, the motor occupation of dimers in the vicinity (upstream and downstream) of the point defect is lower than in the intact lattice. Since we are not considering
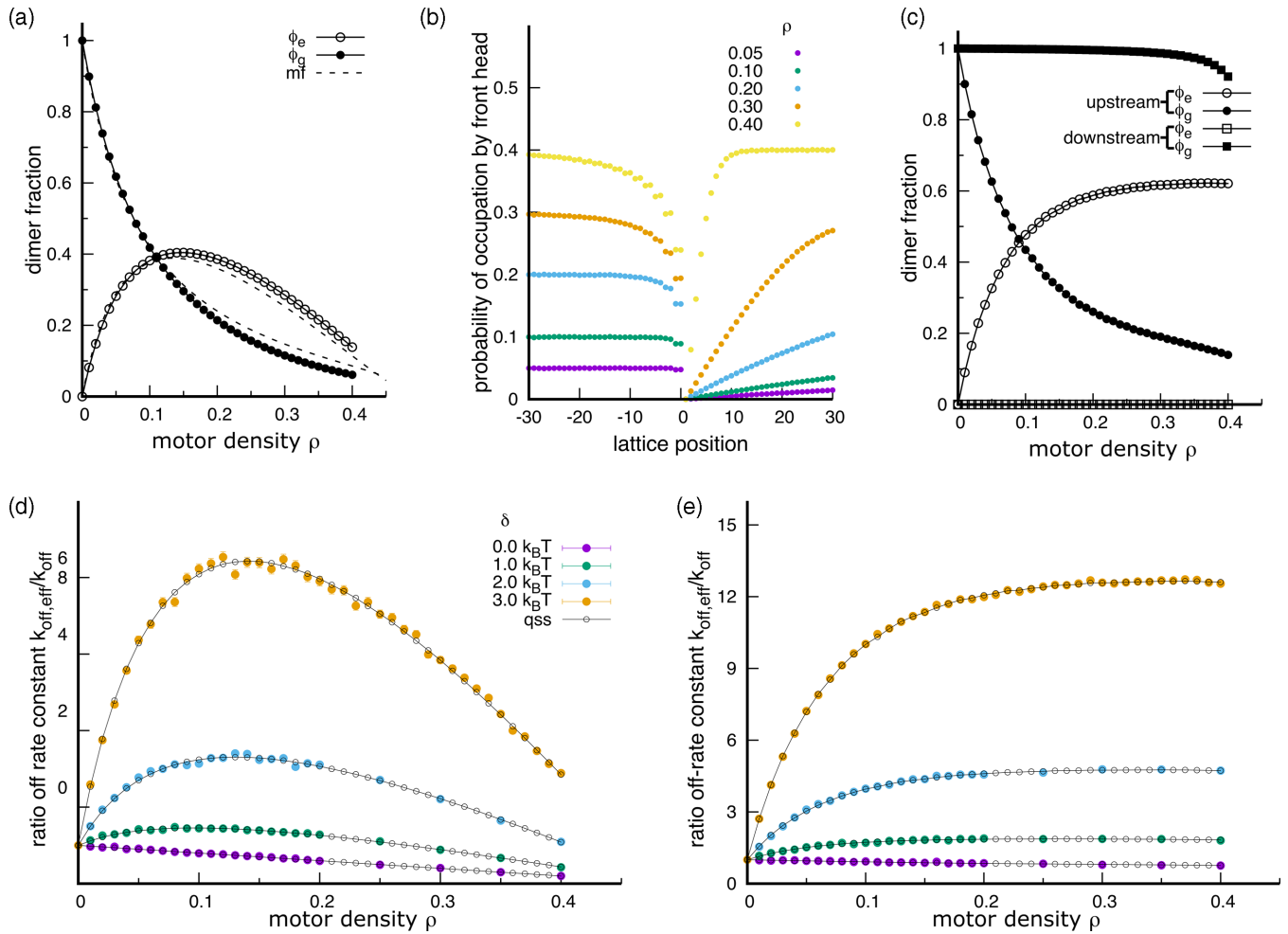
FIG. 2. Effect of motor walk (fast motors) on the stability of the MT shaft in the absence of free tubulin. (a) Quasi-steady-state fractions of excited (ϕ_e) and ground-state dimers (ϕ_g) in the intact lattice depending on the steady-state density of motors, ρ. In the legend, "mf" indicates the mean-field estimate as given in Eqs. (2) and (3). (b) Quasi-steady-state probabilities to find a motor front head in the vicinity of a point defect located at the dimer position $i = 0$ for various steady-state motor densities ρ far away from the defect as indicated in the legend. The motors walk into the positive x direction. (c) Quasi-steady-state fractions of excited and ground-state dimers at a lattice position adjacent to the point defect (upstream). The legend is as in (a). (d) Effective off-rate constant for the creation of a vacancy (normalized by the off-rate constant of the unperturbed lattice) depending on the motor density ρ for various values of the lattice excitation δ as indicated in the legend. (e) Effective off-rate constant for a tubulin dimer upstream of a vacancy (normalized by the off-rate constant of the unperturbed lattice) depending on the motor density ρ of the unperturbed lattice for various values of the lattice excitation δ as indicated in the legend in (d). The (very small) error bars in (d) and (e) correspond to the standard error of the mean (SEM). The axis label "motor density ρ" in (c) and (e) indicates the motor density which would be reached in the intact lattice. Remaining parameters are $k_w = 100\tau^{-1}$, $k_- = 1\tau^{-1}$, and as given in Table I.

sidestepping motors, the motor flux on protofilaments adjacent to the point defect is not affected. Figure 2(c) shows the fraction of excited and ground-state dimers which can potentially leave the lattice immediately upstream and downstream (with respect to the walking direction of motors) to the point defect depending on the steady-state density of motors. Here we denote by steady-state motor density ρ the corresponding density on the intact lattice without defects and which is reached for dimers far away upstream or downstream from the lattice. Upstream of the point defect, the fraction of excited dimers is increasing monotonously with the steady-state motor density. The fast detachment of the motors at the defect guarantees a finite motor flux even at jamming conditions far away from the defect. The motors barely affect the lattice

immediately downstream of the vacancy, since the motor density is here close to zero.

The weak destabilization of a tubulin dimer by the motor walk and the steric blocking of dimers by the presence of motors modify the rate constant k_{off} for the dimer to detach from the lattice and to create a point defect. Since excitation and relaxation processes and the motor walk are fast compared to the residence time of dimers in the full lattice we can estimate the impact of the motor walk on the lattice using a quasi-steady-state assumption

$$k_{off,eff} = k_{off}(\Delta G_b)[\phi_e e^{\beta\delta} + \phi_g], \quad (5)$$

where k_{off} denotes the dimer off-rate constant in the absence of motors; ϕ_e and ϕ_g are determined by the motor speed k_w and

the lattice relaxation rate constant k_r. Figure 2(d) shows the effective rate constant of dimer removal $k_{off,eff}/k_{off}$ depending on the steady-state motor density for kinesin motors and a fast lattice relaxation ($k_w/k_r = 10$, implying that at low motor density each motor walks with a trail of ten excited dimers in its wake) for various values of the motor-inflicted tubulin dimer destabilization values δ. Motors, which do not destabilize the lattice ($\delta = 0$), have a slightly stabilizing effect, due to sterically blocking the dimers from leaving the lattice. However, a small transient perturbation of the lattice as small as $\delta = 3k_B T$ leads to a tenfold increase in the off-rate constant for moderate motor lattice occupations of $\rho = 0.1$ (note that $\rho = 0.5$ indicates a lattice completely saturated with motors, each attached with two heads to two adjacent dimers).

Using slower walking dynein motors and maintaining a fast lattice relaxation ($k_w/k_r = 1$) we obtain qualitatively the same results; however, higher energy penalties δ are needed to produce the same effect as fast walking motors, since the density of excited dimers is lower (see Fig. 7). Interestingly, for slow motors, the effect of the motor walk on the off-rate constant of dimers located upstream of the vacancy is stronger than on the off-rate constant of dimers located in the intact lattice [cf. Figs. 7(d) and 7(e)]. Note that we do not consider side- or backstepping of motors. This assumption is valid for kinesin 1 [44–46]. In contrast, dyneins are known to side- and backstep frequently (10–20 % of steps are side or back steps [40,42,44]), which may quantitatively affect the motor flow and therefore the excitation of dimers. However, simulations for slow motors with 20% backward steps show only minor differences in the excitation state of dimers in the absence and presence of defects [cf. Figs. 7(a) and 7(c)].

Once a point defect has been created, its effects on the microtubule lattice dynamics are twofold:

(i) Neighboring dimers are missing a lateral or longitudinal neighbor and therefore dimer detachment is accelerated.

(ii) The point defect serves as an obstacle for the motor walk, altering the quasi-steady-state value of ϕ_e and ϕ_g and consequently the effective off-rate constant of dimers upstream of the defect, while the dimers downstream of the defect are depleted of motors.

Therefore, a point defect affects the nearest-neighbor dimers in three different ways. Lateral dimers [top and bottom neighbors to the defect in Fig. 1(c)] experience an unperturbed motor flow and may leave the lattice with an effective off-rate constant given by Eq. (5) with the dimer fractions ϕ_g and ϕ_e as given in Fig. 2(a). Longitudinal neighbors upstream of the point defect [left neighbor to the defect in Fig. 1(c)] leave the lattice with an effective off-rate constant given by Eq. (5) with the dimer fractions ϕ_g and ϕ_e as given in Fig. 2(c). Longitudinal neighbors downstream of the point defect [right neighbor to the defect in Fig. 1(c)] are barely affected by the presence of motors and detach from the lattice with the off-rate constant given by Eq. (5) with $\phi_g \approx 1$ and $\phi_e \approx 0$.

B. Microtubule fracture in the absence of free tubulin

In the absence of free tubulin a point defect will lead to the loss of more dimers and a hole will expand longitudinally and laterally along the shaft, until the MT breaks completely (i.e., the hole spans over all 13 protofilaments of the MT). We

define as the time to fracture the time between the creation of a single vacancy and the moment the MT separates into two distinct parts. Similarly we define the length of fracture as the longitudinal extension of the hole at the moment of complete MT fracture.

Due to the lattice anisotropy (longitudinal bonds are assumed to be stronger than lateral bonds), the damaged region will predominantly expand in a longitudinal direction.

Using a total typical lattice binding energy of $\Delta G_b = -45k_B T$ [22] and a MT length of 10 μm corresponding to the approximate length of MTs used in fracture experiments [14], the typical time for the creation of a point defect is of the order of 10 min in the absence of motors and drops, for example, to 3 min in the presence of kinesin motors [$\rho = 0.15$, $\delta = 2k_B T$; see Fig. 3(a)]. Figure 3(b) shows the time to fracture (after creation of a single vacancy) in the presence of fast motors with various energy penalties δ. In the absence of motors, the time to fracture is about 3.5 min. At $\delta = 0$ motors are stabilizing the lattice and the time to fracture increases compared to the motor-free case. However, a small energy penalty ($\delta = 2k_B T$) decreases the time to fracture significantly at low motor densities. However, the dependence is nonmonotonous; i.e., at high motor densities the time to fracture is again increasing. Figure 3(c) shows the length of the damaged region in the shaft at fracture. In the absence of motors the typical damage size at fracture is about 6 μm. In the presence of motors, at $\delta = 0$ the fracture length increases monotonously, i.e., the damage spreads faster in the longitudinal direction than in the lateral direction, compared to the case without motors. A small energy penalty δ leads at low motor densities to a small decrease of the fracture length; at high motor densities the fracture length increases. Overall, the energy penalty δ does not much affect the damage size at fracture. The numerical results (time to fracture, size of damage at fracture) are comparable to experiments (see Fig. 2 in Ref. [14], Supplemental Fig. 4 in Ref. [11]).

Typically in experiments, the effect of motors on the MT stability of end-stabilized MTs in the absence of free tubulin is presented as survival curves, i.e., the fraction of MTs present depending on time. In these experiments, various effects contribute to the MT destruction besides the nucleation of point defects in the intact shaft. For example, the loss of the stabilizing cap and the subsequent rapid MT depolymerization is a major cause of MT destruction. For pedagogical reasons, although the cap loss is not described in our model, Fig. 3(d) shows survival curves of MTs of 10 μm length in the presence of fast walking motors with an energy penalty $\delta = 2k_B T$ for various motor densities. At low motor densities the curves shift to the left; i.e., motors lead to a faster destruction of MTs as observed experimentally in Ref. [14]. However, at high motor densities MTs have the same stability as in the absence of motors, reflecting the nonmonotonous behavior already evident in Fig. 3(b). Note that the typical time of survival is given by the convoluted sum of the probability distributions for the vacancy nucleation and the increase of the defect size up to complete fracture. Putting in numbers, in the absence of motors, the nucleation time for a vacancy in 10-μm-long MTs in the absence of motors is $\approx \frac{1}{0.009 \frac{1}{\mu m\,min} \times 10\,\mu m} = 11$ min [Fig. 3(a), the point where all curves cross the ordinate].
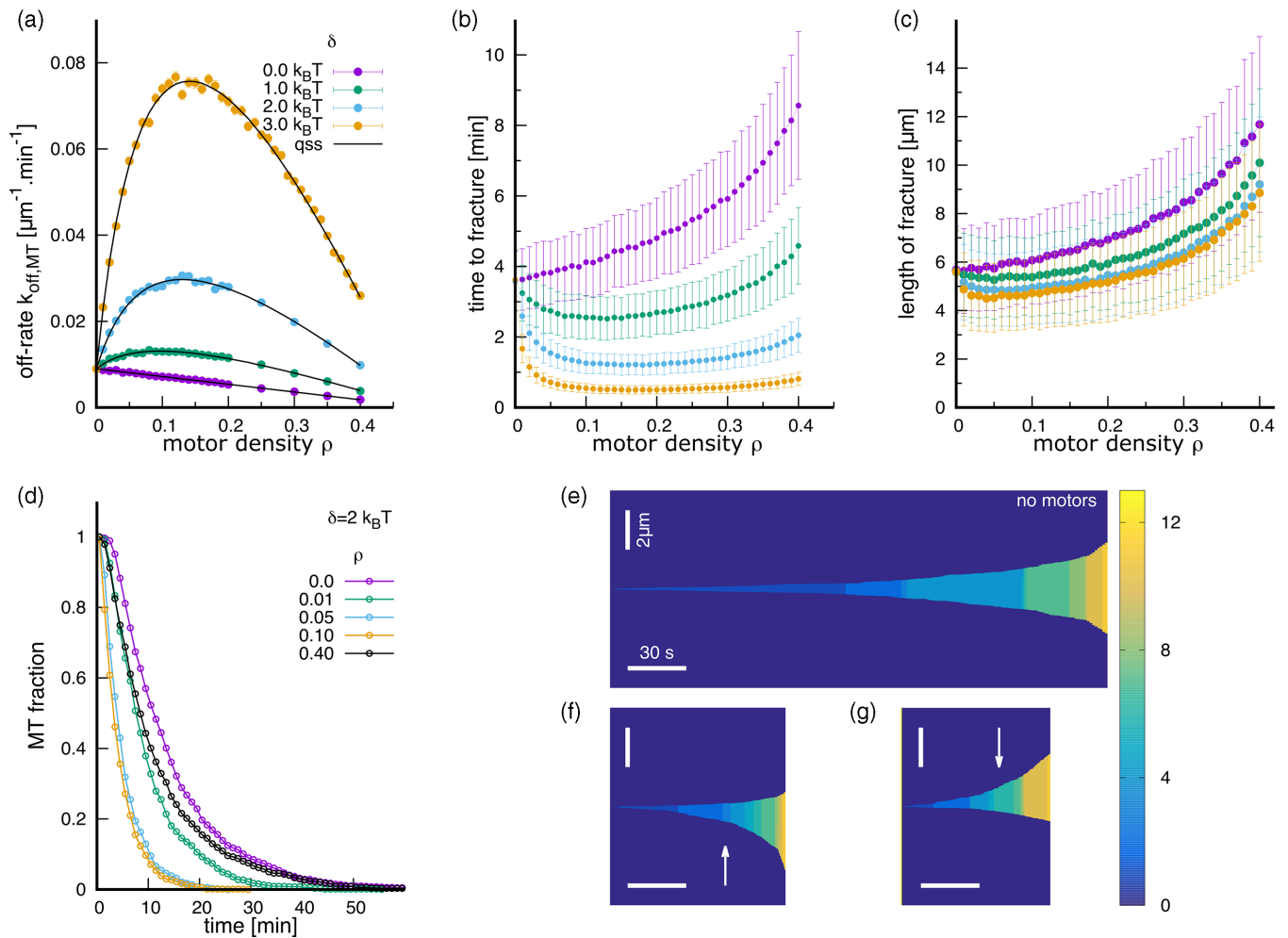
FIG. 3. Effect of motor walk on the fracture of the MT shaft. (a) Effective rate constant for the creation of a vacancy per micrometer MT length depending on the motor density ρ for various values of the lattice excitation δ for fast motors as indicated in the legend. The (small) error bars represent the SEM. (b) Time to fracture and (c) length of damaged region at fracture after the creation of a vacancy depending on the motor density ρ for various values of the lattice excitation δ for fast motors as indicated in the legend in (a). The error bars represent the standard deviation (SD). (d) Survival curves of MTs (of 10 μm length) for various values of the motor density ρ for $\delta = 2k_BT$ for fast motors. Kymographs of the fracture process in (e) the absence of motors and [(f), (g)] the presence of (+)- and (−)-end directed motors. Shown is the position along the MT (vertical axis) versus time (horizontal axis). The color code corresponds to the number of fractured protofilaments. Simulations were started with a point defect in the center of the MT on protofilament 6 (opposite of the seam). The direction of motor walk is indicated by the white arrows. Remaining parameters are (f) $k_w = 100\tau^{-1}$, $k_- = 1\tau^{-1}$, $\rho = 0.1$, $\delta = 2k_BT$ and (g) $k_w = 10\tau^{-1}$, $k_- = 0.1\tau^{-1}$, $\rho = 0.05$, $\delta = 4k_BT$ and as given in Table I.

The typical time for the damaged region to spread across all protofilaments is about 3.5 min [Fig. 3(b)]. Summing up gives a typical time of survival of 14.5 min, which corresponds to the magenta curve in Fig. 3(d). Doing the same calculation for a motor density of $\rho = 0.1$ and a penalty of $\delta = 2k_BT$ we have a typical vacancy nucleation time of $\approx \frac{1}{0.03 \frac{1}{\mu m \, min} \times 10 \, \mu m} = 3.3$ min and a time to complete fracture of about 1.2 min, which gives a typical survival time of 4.5 min corresponding to the orange curve in Fig. 3(d).

Finally, Fig. 3(e) shows three kymographs of MT fracture in the absence and presence of motors. In the absence of motors, the damage spreads symmetrically in the longitudinal direction. Defect growth in the longitudinal direction is faster than in the lateral direction. The defect growth speed in the longitudinal direction increases with the size of damage in

the lateral direction. When the last intact protofilament loses a dimer, fracture is complete. In the presence of (+)-end directed motors the most obvious effect is that the damage spreads faster towards the (−) end than the (+) end, since motors walking towards the point defect are destabilizing the dimers upstream to the existing damage. The downstream side of the damage is not affected by the motors [i.e., the fraction of excited dimers downstream of the damage is vanishing due to a depletion of motors in this region; see Figs. 2(b) and 2(c)]. The difference between the upstream and downstream front propagation of the defect is shown in more detail in Fig. 8. Note also the difference in the timescale on which fracture occurs; for the chosen example motors accelerate fracture two- to threefold compared to the case without motors. In the presence of (−)-end directed motors the damage spreads

faster towards the (+) end than the (-) end. For completeness, Fig. 9 shows the equivalent of Figs. 3(a)–3(c) for slowly walking (−)-end directed motors.

In a final set of calculations we have studied the dynamics of a point defect in the presence of free tubulin dimers at high concentration.

C. Vacancy dynamics in the presence of free tubulin dimers

In the absence of any steric constraints in the lattice, a single point defect will be occupied by a newly incorporated dimer with a typical time $\tau_{\mathrm{on}} = (k_{\mathrm{on}}c)^{-1} = 0.05$ s (for a concentration of free tubulin $c = 20 \, \mu$M and the k_{on} rate constant given in Table I). Conversely, a GDP dimer sitting next to a vacancy in a longitudinal direction will leave the lattice with a typical time $\tau_{\mathrm{off}} = [k_{\mathrm{off}}^* e^{\beta(\Delta G_1 + 2\Delta G_2 - \Delta G^*)}]^{-1} = 3.3$ s $\gg \tau_{\mathrm{on}}$ (see Table I). Therefore, any point defect appearing in the lattice should be closed immediately in the presence of free tubulin, after which the lattice is repaired completely.

This picture changes completely if we assume that a GTP-tubulin dimer experiences a steric hindrance to incorporate the GDP lattice at a single point defect. Both GMPCPP tubulin (a slowly hydrolyzing analog of GTP tubulin) and GDP tubulin are assumed to adopt a curved conformation in solution albeit with different curvature [47–49], which needs to straighten to integrate a tube lattice. A recent kinetic study of the MT tip dynamics [50] proposes a scenario based on steric constraints, where GTP tubulin integrates the MT tip with an energetic preference for a so-called bent conformation to form a sheet structure. Upon GTP hydrolysis the conformation of GDP tubulin shifts towards a straight conformation to close the sheet into a tube structure. In this scenario a GTP tubulin from solution would be in an unfavorable conformation to integrate a point defect in a GDP lattice existing in a straight tube conformation. Furthermore, structural studies [30,51,52] on MT tube structures using analogs for GTP tubulin and slowly hydrolyzing mutant tubulins show a high sensitivity of structural properties of the microtubule (longitudinal and lateral interdimer distances, preferred protofilament number, and lattice skew and twist) with respect to the type of tubulin dimers that form the lattice. Another interesting observation stems from the dynamical behavior of MTs polymerized from mixtures of GTP and GDP tubulins [53,54]. These MTs depolymerize significantly slower than MTs formed from pure GTP tubulin, indicating structural differences between MTs arising from different polymerization conditions.

Here, in our simple MT-lattice model, we explore the consequences of these structural incompatibilities under the hypothesis that neither GTP tubulin nor GDP tubulin (most probably present in low concentrations in the experiments) can integrate a point defect in a GDP-lattice environment existing in a straight tube conformation [55]. Thereby we consider a point defect with two lateral GDP neighbors as a GDP-lattice environment [see Fig. 4(a)]. This assumption creates a lattice dynamics in the neighborhood of the vacancy, which can potentially survive an extended period of time and lead to localized tubulin exchange experimentally visible in fluorescence microscopy [14–16]. Due to the high anisotropy of the lattice the vacancy will perform a random walk predominantly along a single protofilament, i.e., up or down the MT axis. In this mechanism, a longitudinal neighbor of a single point defect will leave the lattice, creating a double point defect allowing a free GTP-tubulin dimer to attach to one of the two vacant sites. After this cycle of detachment and attachment the lattice has again a single point defect.

Figure 4(b) shows example trajectories over 15 min in the absence of motors, and with (+)- and (−)-end directed destabilizing motors. In the absence of motors, the vacancy dynamics is slow and covers only a small distance on the protofilament $\leqslant 0.25 \, \mu$m. The trajectories are mainly diffusive, i.e., $\langle x^2 \rangle \sim t$, and get slightly superdiffusive at long times, due to the stabilizing effects of GTP contacts in the lattice and the asymmetry in the GTP hydrolysis [see Figs. 4(b) and 4(c)]. Therefore, the vacancy migrates slowly towards the MT (+) end.

However, in the presence of destabilizing walking motors, the vacancy trajectories are accelerated and become ballistic at long times; i.e., the vacancies are drifting and the mean-squared displacement behaves as $\langle x^2 \rangle \sim t^2$. The drift direction depends on the walking direction of the motors; (+)-end directed motors induce a drift towards the MT (−) end, and (−)-end directed motors induce a drift towards the MT (+) end. Thereby, the dynamics is crucially determined by the following factors: the motor penalty δ and the off-rate constant of the tubulin dimers immediately upstream or downstream of the point defect (influenced by the dimer fractions ϕ_{e} and ϕ_{g}).

For a motor penalty $\delta = 0$ the tubulin dimer situated upstream of the vacancy is slightly stabilized [see Fig. 2(e)]. In the case of the (+)-end directed motor, this small effect reinforces the inherent small bias of the vacancy to drift towards the MT (+) end [increased mean squared displacement (MSD) in Fig. 4(c) for (+)-end directed motors with $\delta = 0$]. For (−)-end directed motors with $\delta = 0$, the stabilizing effect by the motors induces a small drift of the vacancy towards the MT (−) end, which is competing with the inherent drift of the vacancy towards the MT (+) end due to GTP hydrolysis [decreased MSD in Fig. 4(c) for (−)-end directed motors with $\delta = 0$].

As an illustration Fig. 4(d) shows example kymographs of tubulin exchange, where dimers directly incorporated into the shaft are shown in yellow. Figure 4(e) shows the length of incorporation spots depending on the motor concentration and energy penalty δ for fast (+)-end directed and slow (−)-end directed motors. Without motors at $\rho = 0$ the incorporation length is about $0.25 \, \mu$m. Without motor walk induced penalty ($\delta = 0$) this length barely changes. However, at a small penalty of $\delta = 1k_{\mathrm{B}}T$ (fast motors) the incorporation length increases to about $1 \, \mu$m at high motor density ($\rho = 0.2$). For $\delta = 2k_{\mathrm{B}}T$ (fast motors) the incorporation length increases strongly with the motor density. Even at a low motor density ($\rho = 0.02$) the incorporation length is about $1 \, \mu$m. Slow motors have a similar effect as fast motors, albeit at higher energy penalties δ. For comparison, in experiments the incorporation length after 7–40 min of tubulin incorporation with kinesins (fast motors in our model) is approximately $1 \, \mu$m [14–16].

So far, we have investigated a vacancy dynamics without considering possible repair mechanisms, which could lead to the closure of a point defect. As a weak assumption we
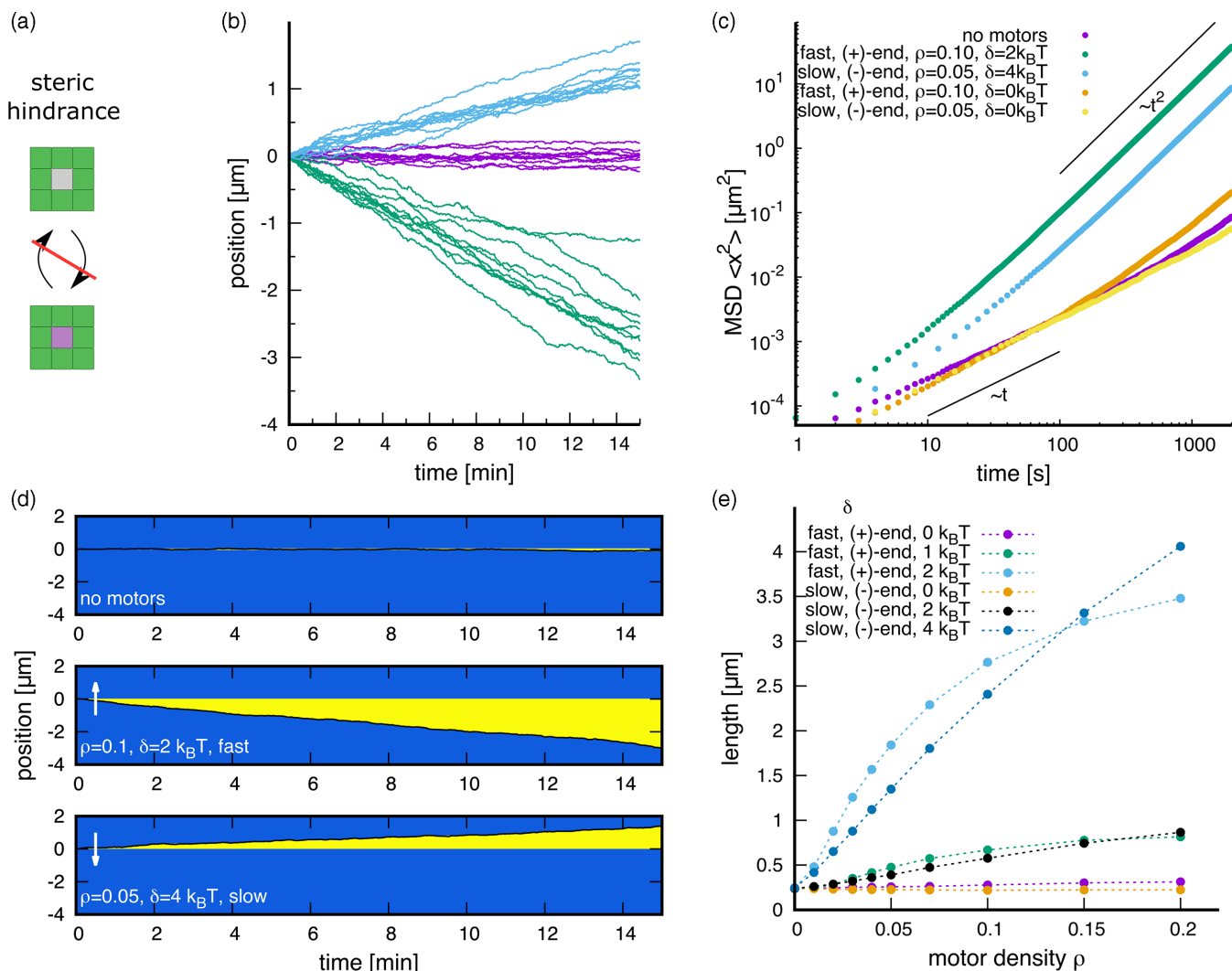
FIG. 4. Effect of motor walk on the dynamics of a point defect in the presence of free tubulin. (a) GTP-tubulin dimers (pink) cannot leave or integrate a fully occupied GDP lattice (green) with a single point defect (gray) due to steric hindrance. (b) Example trajectories of point defects in the absence and presence of motors along a protofilament as indicated in the legend in (c). (c) Mean squared displacements of point defect trajectories for various motor properties as indicated in the legend. (d) Examples of kymographs of tubulin exchange (yellow). The current position of the point defect corresponds to the black line. The direction of motor walk is indicated by the white arrow. (e) Length of tubulin exchange after 15 min depending on the motor density ρ for fast (+)-end directed and slow (−)-end directed motors for various energy penalties δ as indicated in the legend. Parameters for fast motors are $k_{\mathrm{w}} = 100\tau^{-1}$, $k_{-} = 1\tau^{-1}$, and for slow motors $k_{\mathrm{w}} = 10\tau^{-1}$, $k_{-} = 0.1\tau^{-1}$ and as given in the legends and in Table I. The concentration of free tubulin is $c = 20\ \mu\mathrm{M}$.

could postulate that a lateral GTP-tubulin dimer adjacent to a vacancy allows for the incorporation of a free GTP-tubulin dimer, since the GTP dimer already present in the lattice sufficiently extends the vacancy site to allow for a GTP dimer to incorporate. In this picture, a point defect repairs completely, as soon as a vacancy loses a lateral GDP-dimer neighbor. In the absence of motors, the typical lifetime of a point defect is then given by $\tau_{\mathrm{L}} = [k_{\mathrm{off}}^{*} e^{\beta(2\Delta G_1 + \Delta G_2 - \Delta G^*)}]^{-1} = 100$ min, well beyond the observation time in an experiment. In the presence of destabilizing walking motors, the lifetime may shorten considerably [cf. Fig. 2(d)]. For example, an effective increase in the off-rate constant for a lateral dimer by a factor of 3 [Fig. 2(d), $\rho = 0.15$, $\delta = 2k_{\mathrm{B}}T$] reduces the lifetime of the vacancy to $100/3$ min $= 33$ min, which is comparable to the experimental timescale.

A second potential repair mechanism of point defects could result from relaxing the rule of steric constraint for the inclusion of free tubulin at point defects, i.e., allowing for an on-rate constant $\sim\zeta k_{\mathrm{on}}$ with $\zeta \ll 1$. Repair would then be complete with a typical time $\sim 1/(\zeta k_{\mathrm{on}})$.

IV. DISCUSSION

In the present paper we have theoretically explored a possible mechanism for MT lattice plasticity in the presence of processive molecular motors. Our basic idea is that the motor walk transiently, locally, and weakly destabilizes the underlying MT lattice, which increases the rate of tubulin dimer loss from the shaft lattice. Assuming a steric hindrance for GTP-tubulin dimers to integrate a single vacancy in the

GDP lattice induces a lattice dynamics at the vacancy which is accelerated by molecular motors. Furthermore, the vacancy dynamics switches from diffusive to ballistic in the presence of motors whereby the direction of motion depends on the direction of the motor walk.

The proposed model mechanism matches qualitatively and quantitatively fracture experiments (fracture size and time to fracture) of end-stabilized MTs in the absence of free tubulin dimers. It is also consistent with experiments on end-stabilized MTs in the presence of free tubulin dimers, which show an increase in the frequency of free dimer incorporation spots with typical sizes of about 1 μm.

Frequencies of incorporation spots have been measured by two different groups and vary considerably. Andreu-Carbó *et al.* [16] measured a frequency of 0.05 μm^{-1} after 15 min of free tubulin incorporation in the absence of motors. In the presence of kinesins (5 nM), the frequency increased to 0.2 μm^{-1}, which is consistent with defect nucleation rates shown in Fig. 3(a). In contrast, Triclin *et al.* [14] measured frequencies of 0.017 μm^{-1} after 40 min of free tubulin incorporation in the absence of motors. In the presence of kinesins (10 nM), the frequency of incorporation increased to 0.05 μm^{-1}, which is lower by a factor of 4 than the frequency measured by Andreu-Carbó *et al.* [16] at much shorter incubation times. While the absolute frequency of incorporation may depend on the sensitivity of the experimental setup, both groups find an increase in the incorporation frequency in the presence of motors by a factor of 3 to 4 compared to the control experiment, which corresponds in our model to a motor penalty of about $2k_BT$ or slightly above for low kinesin densities on the MT.

A recent paper by Théry and Blanchoin [56] speculates about possible mechanisms of interaction between the processive motor walk and the underlying MT lattice. They juxtapose two different concepts: the motor facilitates the lattice dynamics at dislocations (e.g., changes in protofilament numbers) (termed the "pickpocket" and "burglar" concept, respectively) as opposed to the idea that the motor weakly destabilizes the perfect lattice in its wake (termed the "road-burner"). In the first case, the motor walk acts on existing defects, which were created during polymerization. In the latter case, the motor continuously and weakly perturbs the lattice which leads to the nucleation of vacancies.

Here we have investigated the "road-burner" concept where MT shaft plasticity is enhanced as a collective motor effect; the motor walk weakly destabilizes the MT lattice on an energy scale of a few k_BT and facilitates detachment of dimers from the lattice. The dynamics of an existing vacancy is greatly accelerated upstream of the motor current, whereas downstream of the vacancy the lattice is devoid of motors, leading to a vacancy drift in a direction opposite of the walking direction. Both concepts (i.e., motors act on existing defects and nucleate new defects) are not mutually exclusive and could act in an additive manner. However, the road-burner concept (*de novo* nucleation) would increase the number of sites of lattice plasticity depending on the motor density present on the MT [16], offering a true mechanism of MT regulation.

An important feature in motor-induced MT lattice dynamics is the motor behavior at lattice vacancies. In the

here proposed model mechanism, motor-stimulated dimer removal upstream of vacancies requires a sufficiently high motor flux. In our simulations we had only considered motors which walk on single protofilaments and detach rapidly at the vacancy. However, especially dyneins are known to sidestep frequently. In the vicinity of vacancies this might be an important alternative mechanism to maintain a high motor flux and reduce jamming upstream of the vacancy.

It was suggested in Ref. [21] that the walk of a single kinesin is sufficient to directly remove dimers from the MT shaft as a rare event. Indeed, the experiments in Ref. [21] show that the cooperative action of several kinesins may be able to remove a tubulin dimer from the lattice by pulling on the dimer via a flexible tether, although a direct proof of dimer removal is missing. Within this concept of direct dimer removal, the motor walk facilitates vacancy nucleation, as an extremely rare event. It is not clear how the motors affect the lattice in the vicinity of the vacancy, since this would require that a rare lattice destabilization event occurs at an existing vacancy. A direct dimer removal offers therefore no straightforward explanation for micrometer-sized tubulin incorporation spots, which involve an exchange of several tens to 100 dimers length. However, the direct detachment of tubulin dimers by the kinesin walk as a rare event can be treated potentially within the same kinetic Monte Carlo framework we have used here. To that end, only an almost vanishing small fraction of motor steps leads to a strong transient lattice destabilization (limited by the free energy of ATP hydrolysis). An investigation of this "single-molecule" mechanism with respect to MT fracture and free tubulin incorporation is part of future work in an attempt to oppose the two mechanisms of motor-lattice interactions.

It has been speculated that GTP islands in the GDP shaft may serve as rescue sites for rapidly depolymerizing MTs and thus an increased tubulin turnover in the shaft may entail an increased MT stability. Indeed, it has been shown *in vivo* and *in vitro* that an increased frequency of tubulin exchange sites correlates with a higher rescue frequency [16,57,58]. Increasing the stability of dynamic MTs by increasing the MT shaft plasticity constitutes a completely novel and unexplored mechanism of MT regulation, of which a mechanistic picture is completely missing. Our proposed mechanism for MT-motor interactions could serve as an important cornerstone in plasticity-induced MT regulatory mechanisms.

Data and source codes for Figs. 2(a)–2(e), 3(a)–3(d), 4(b), 4(c), 4(e), 5, 7(a)–7(e), 8, and 9(a)–9(c) are available on the Zenodo repository [59].

APPENDIX: MODEL DETAILS AND SUPPLEMENTARY FIGURES

Kinetic Monte Carlo simulations were performed using a rejection-free random-selection method [60], and using custom written codes in C and PYTHON. Statistical analysis (averages, standard deviations, and standard errors of the mean) was either performed using C, PYTHON, or R. Unless stated otherwise, kinetic Monte Carlo simulations were performed using the parameters shown in Table I.

a. Details of the seam structure. Individual lattice sites on the square lattice are identified by a doublet of integers (i, j). Lattice sites at the seam have two nearest lateral "half" neighbors across the seam; that is, dimers at the seam in Fig. 1(a) with the doublet $(1, j)$ are in contact with dimers $(13, j + 2)$ and $(13, j + 1)$ at the opposite site of the seam and dimers at the right seam with doublet $(13, j)$ are in contact with dimers $(1, j - -1)$ and $(1, j - -2)$ for a 13_3 protofilament lattice. Each lateral dimer-dimer contact across the seam is counted with a binding energy $\Delta G_2/2$; i.e., in the fully occupied lattice, dimers at the seam have the same binding energy as dimers in the bulk lattice.

b. Principle of detailed balance for reversible reactions. For the passive process of lattice polymerization and depolymerization, the principle of detailed balance has to hold.

Therefore, on- and off-rate constants, k_{on} and k_{off}, must be coupled by the relation [61]

$$\frac{k_{\mathrm{off}}}{k_{\mathrm{on}} c_0} = e^{\beta \Delta G}, \tag{A1}$$

where $\beta^{-1} = k_{\mathrm{B}}T$, c_0 denotes the standard concentration of free tubulin in solution, that is, 1 M by convention, and ΔG denotes the change in free energy upon transferring a free dimer from the solution into the lattice. Note that c_0 in Eq. (A1) is not the actual concentration of the free tubulin in solution, but the standard concentration, and originates from the concentration dependence of the chemical potential, that is, $k_B T \ln(c/c_0)$, where c denotes the actual concentration of free tubulin in solution. $\Delta G = \Delta G_{\mathrm{b}} + \Delta G_{\mathrm{e}} + \delta$ contains contributions from binding of the dimer to nearest neighbors ΔG_{b}, the loss of entropy due to immobilization of the free dimer in the lattice ΔG_{e}, and an additional (weak) transient contribution δ due to the stepping of processive motors. We rewrite Eq. (A1) into

$$k_{\mathrm{off}} = k_{\mathrm{on}} c_0 e^{\beta \Delta G} = k_{\mathrm{off}}^* e^{\beta(\Delta G_{\mathrm{b}} + \delta - \Delta G^*)} \tag{A2}$$

with $k_{\mathrm{off}}^* = k_{\mathrm{on}} c_0 e^{\beta(\Delta G_{\mathrm{e}} + \Delta G^*)}$. $\Delta G^* = \Delta G_1 + \Delta G_1^T + \Delta G_2$ denotes the binding energy at the microtubule tip with a GTP cap (i.e., the binding energy of a GTP dimer with one lateral and one longitudinal GTP-dimer neighbor).

TABLE I. Parameters for the kinetic Monte Carlo simulations unless stated otherwise. T-T (D-D) indicates a contact between GTP dimers (GDP dimers), and T-D indicates a contact between a GTP and GDP dimer. The timescale is $\tau = 1$ s.

| Parameter	Notation	Value	Remark
Binding energies:			Great variability in the values found
Longitudinal (T-D, D-D)	ΔG_1	$-15 k_{\mathrm{B}}T$	in the literature [11,22,23,33,62,63];
Lateral (T-D, D-D)	ΔG_2	$-7.5 k_{\mathrm{B}}T$	lattice anisotropy is $\Delta G_1/\Delta G_2 = 2$
Longitudinal stabilizing (T-T)	ΔG_1^T	$-6.3 k_{\mathrm{B}}T$	
GTP hydrolysis rate constant	k_{h}	$0.6\ \tau^{-1}$	comparable to experimental values [64] and values used in other theoretical studies [11,25,26]
Entropic loss due to dimer immobilization			Estimated from $k_{\mathrm{off}}^* = k_{\mathrm{on}} c_0 e^{\Delta G_{\mathrm{e}} + \Delta G_1 + \Delta G_2 + \Delta G_1^T}$, estimates in the literature range from $10 k_{\mathrm{B}}T$ to $20 k_{\mathrm{B}}T$ [22,65,66]
Reference energy at the MT tip	ΔG^*	$28.8 k_{\mathrm{B}}T$	$\Delta G^* = \Delta G_1 + \Delta G_2 + \Delta G_1^T$
On-rate constant (GTP dimer)	k_{on}	$1\ \mu\mathrm{M}^{-1}\,\tau^{-1}$	Overall on-rate constant per 13 protofilament MT is $k_{\mathrm{on}}^{\mathrm{MT}} = 13\ \mu\mathrm{M}^{-1}\,\tau^{-1}$, comparable to other studies [3,22,23,64]
Off-rate constant	k_{off}^*	τ^{-1}	Corresponds to the off-rate constant for a GTP Corresponds to the off-rate constant for a GTP dimer with one lateral and longitudinal GTP neighbor
Motor speed	k_w	$10\tau^{-1}$–$100\tau^{-1}$	Comparable to typical speeds for yeast dyneins (10 dimers/s) or kinesins (100 dimers/s) [15,40,67,68]
Motor off-rate constant	k_-	$0.1\tau^{-1}$–$1\tau^{-1}$	$k_- = 0.1\tau^{-1}$ with $k_w = 10\tau^{-1}$ and $k_- = 1\tau^{-1}$ with $k_w = 100\tau^{-1}$ corresponds to a typical run length of 100 dimers, comparable to experiments on dyneins and kinesins [15,40,67,68]
Motor off-rate constant (MT end)	$k_-^{\mathrm{E}} = \theta k_-$	$\theta = 100$	We assume motors are not end tracking [43]
Motor on-rate constant	k_+		Adapted to obtain a steady-state motor density ρ using Eq. (A3)
Conformational penalty due to motor stepping (per dimer)	δ	$0 k_{\mathrm{B}}T$–$4 k_{\mathrm{B}}T$	Adapted for our model
Lattice relaxation time	k_r	$1\tau^{-1}$	Adapted for our model
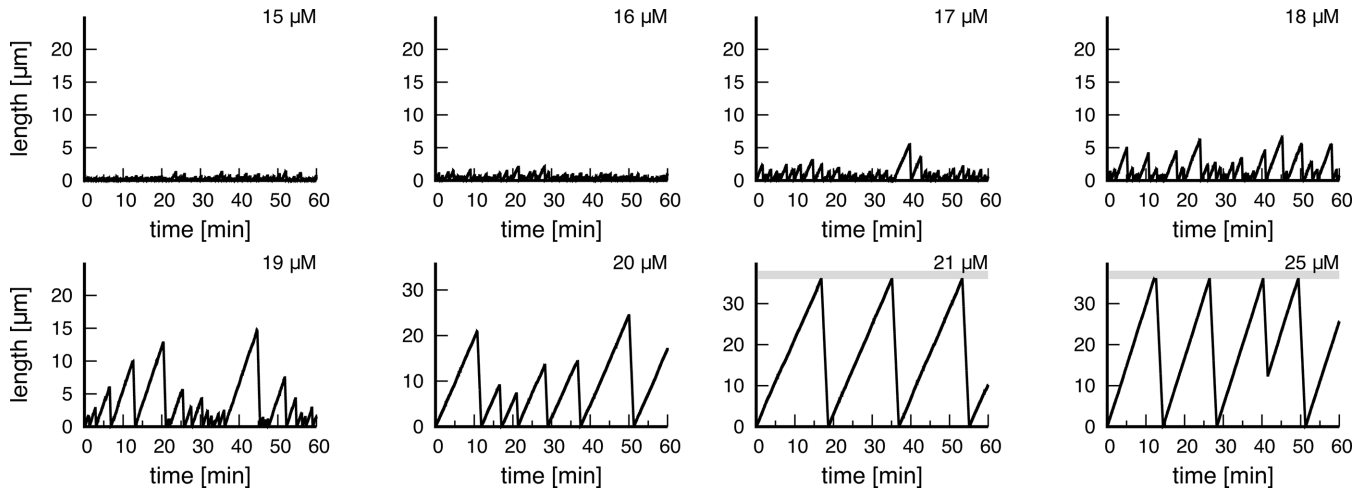
FIG. 5. Tip dynamics of the MTs depending on the concentration of free tubulin as indicated in the upper right corner of each graph. The gray bars for 21 μM and 25 μM denotes the end of the simulation box, which triggers catastrophes. Remaining parameters are as given in Table I.

c. Justification for the choice of ΔG_1^{T}. Note that the stabilization of longitudinal T-T contacts is a major difference from the model by vanBuren *et al.* [22], but permits to capture the dynamic instability without further assumptions. The stabilization of only lateral T-T contacts is not sufficient to induce a dynamic instability with sufficiently long phases of growth and shrinkage.

d. Motor dynamics with occasional backward steps. Figures 7(a) and 7(c) show results for the steady fractions of excited and ground-state dimers which can leave the lattice, ϕ_e and ϕ_g for slow motors which may occasionally step backwards. These simulations were carried out under the assumption that the motor walks with a mean speed $\langle v \rangle = 10\tau^{-1}$. The rate constant for doing a forward step is given by $k_{\mathrm{w,f}} \frac{1-\xi}{1-2\xi}\langle v \rangle$ and the backward-stepping rate constant is $k_{\mathrm{w,b}} \frac{\xi}{1-2\xi}\langle v \rangle$. ξ denotes the fraction of backward steps which is 0.2 in the simulations in Figs. 6(a) and

6(c). The mean velocity $\langle v \rangle$ is related to $k_{\mathrm{w,f}}$ and $k_{\mathrm{w,b}}$ by $\langle v \rangle = k_{\mathrm{w,f}} - k_{\mathrm{w,b}}$.

e. Motor dynamics in the mean-field approximation. Typically, simulations were carried out for a given quasi-steady-state motor density at the intact lattice (i.e., the temporal average of the probability that a motor front head is attached to a tubulin dimer after all transients have decayed). In this situation, the motor (front head) density is related to the motor on-rate constant k_+ and the motor off-rate constant k_- [27,37] by

$$0 = k_+ \frac{(1-2\rho)^2}{1-\rho} - k_-\rho. \tag{A3}$$

For a given ρ and motor off-rate constant k_-, Eq. (A3) determines the motor on-rate constant k_+. The microtubule lattice was initiated with all tubulin dimers in the ground state and with a mean motor density $\approx \rho$. Statistical measures of the lattice dynamics in the presence of motors were recorded after a short period of equilibration $\sim 10 k_-^{-1}$.
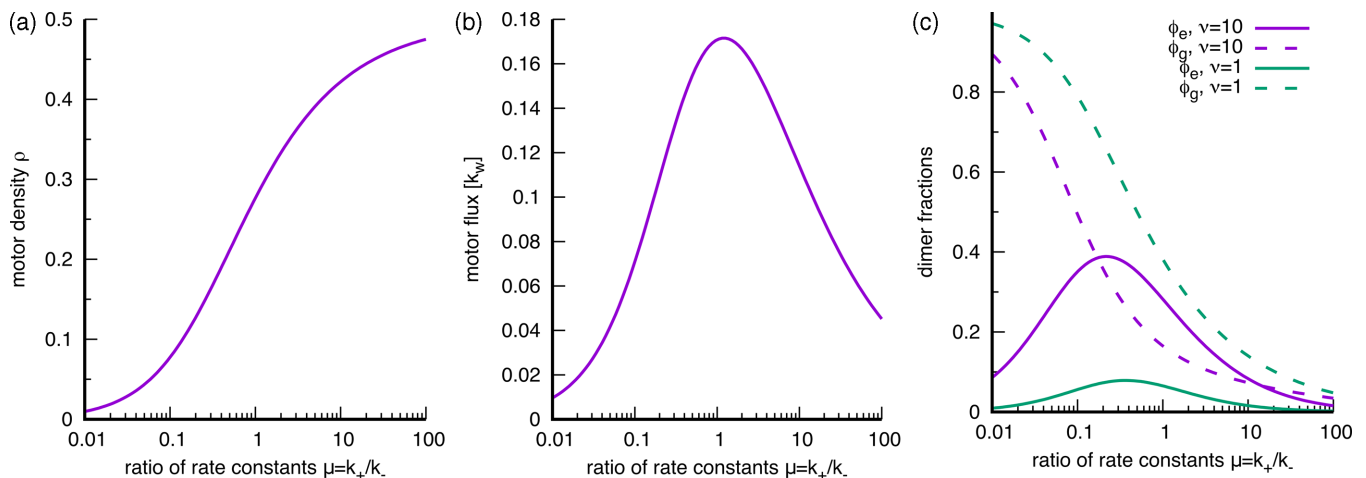

FIG. 6. Steady-state behavior of motors and dimer fractions ϕ_e and ϕ_g depending on the ratio of motor attachment and detachment rate constants $\mu = k_+/k_-$. (a) Steady-state density of motors on the intact lattice according to Eq. (A3). (b) Steady-state flux of motors according to Eq. (4) along an intact protofilament in units of the motor stepping rate constant k_{w}. (c) Approximate fractions of exited (ϕ_e) and ground-state dimers (ϕ_g) for fast ($\nu = k_{\mathrm{w}}/k_{\mathrm{r}} = 10$) and slow motors ($\nu = k_{\mathrm{w}}/k_{\mathrm{r}} = 1$) according to Eqs. (2) and (3).
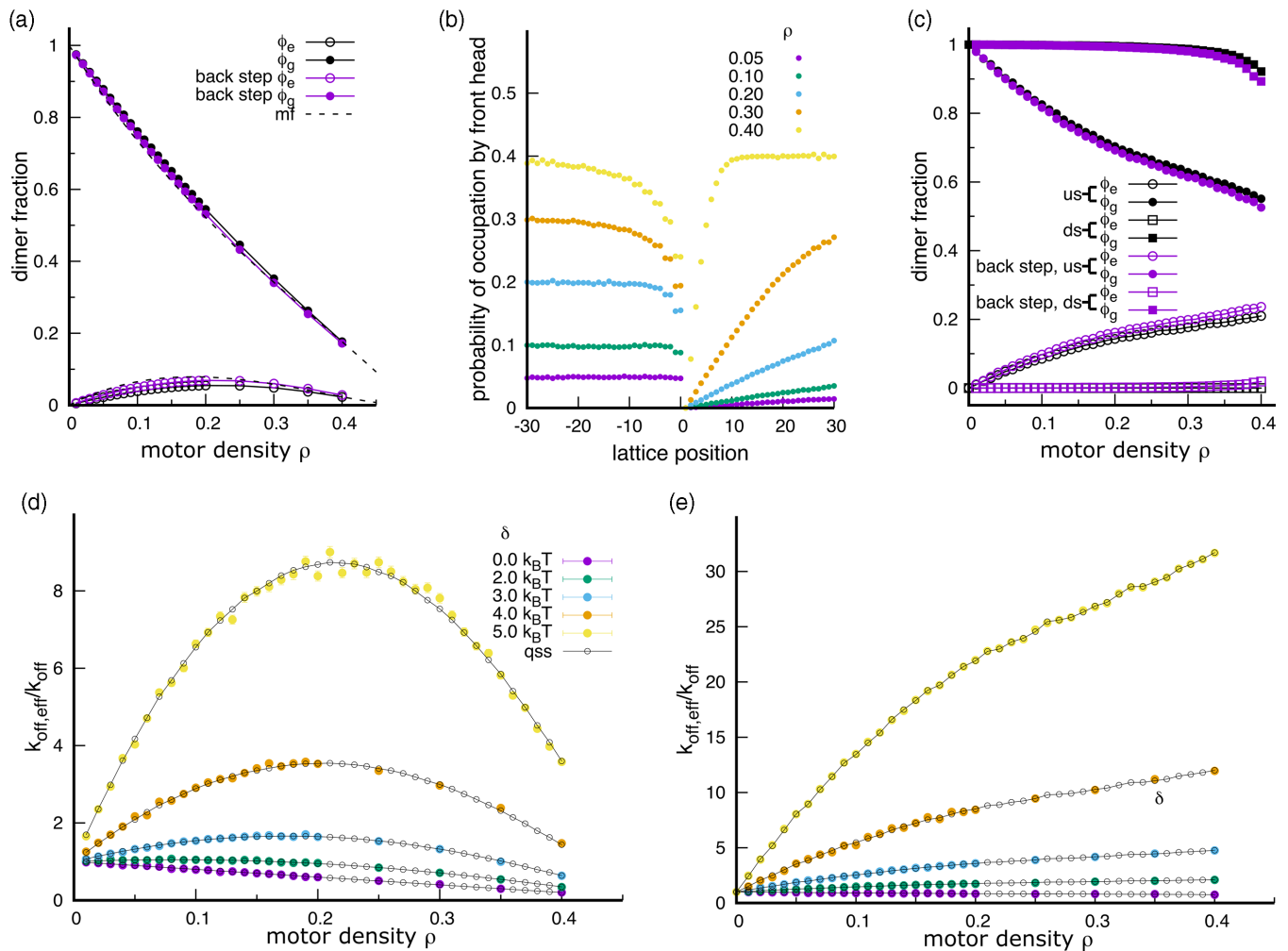
FIG. 7. Effect of motor walk on the stability of the MT shaft for slowly walking motors. (a) Quasi-steady-state fractions of excited (ϕ_e) and ground-state dimers (ϕ_g) in the intact lattice depending on the steady-state density of motors, ρ. "Back step" indicates motors that do 20% backward steps; "mf" indicates the mean-field estimate as given in Eqs. (2) and (3). (b) Quasi-steady-state probabilities to find a motor front head in the vicinity of a point defect located at the dimer position $i = 0$. The motors walk into the positive x direction. (c) Quasi-steady-state fractions of excited and ground-state dimers at a lattice position adjacent to the point defect (us, upstream; ds, downstream). "Back step" indicates motors that do 20% backward steps. (d) Effective off-rate constant for the creation of a vacancy (normalized by the off-rate constant of the unperturbed lattice) depending on the motor density ρ for various values of the lattice excitation δ as indicated in the legend. (e) Effective off-rate constant for a tubulin dimer upstream of a vacancy (normalized by the off-rate constant of the unperturbed lattice) depending on the motor density ρ of the unperturbed lattice for various values of the lattice excitation δ as indicated in the legend in (d). The (small) error bars in (d) and (e) represent the SEM. The axis label "motor density ρ" in (c) and (e) indicates the motor density which would be reached in the intact lattice. Remaining parameters are $k_w = 10\tau^{-1}$, $k_- = 0.1\tau^{-1}$, and as given in Table I.

f. Motor-lattice interactions in the quasi-steady-state approach. The computational effort of the kinetic Monte Carlo (KMC) model presented in the Model section in the main text increases rapidly with the employed motor density since the system dynamics is driven by two different timescales. On the one hand, the tubulin dynamics [$k_{off}^{-1}(\Delta G^*) = 1$ s] is slow, and on the other hand, the motor dynamics ($k_w^{-1} = 0.1$–0.01 s) is one to two orders of magnitude faster. It is then a prerequisite to optimize the KMC algorithm to minimize the computational time. One can either reduce the total number of reactions needed to simulate the system (i.e., reduce the complexity of the model) or increase the number of reactions

per second (i.e., optimize the script algorithm). Some of the simulations (MT fracture) were done with a sharp reduction in the complexity (i.e., the number of considered reactions), using a quasi-steady-state assumption to capture the effect of the motor walk on the lattice stability. To that end we tabulated the steady-state fractions of dimers in the excited and ground states (ϕ_e, ϕ_g) that are able to leave the lattice; i.e., they are not blocked by the presence of motors bound to two dimers. Thereby we considered two cases. In case I the motors move on an intact protofilament with translational symmetry and the steady states are given by (ϕ_e, ϕ_g) = ($\phi_{e,i}$, $\phi_{g,i}$). In case II, we considered a protofilament containing a point defect and
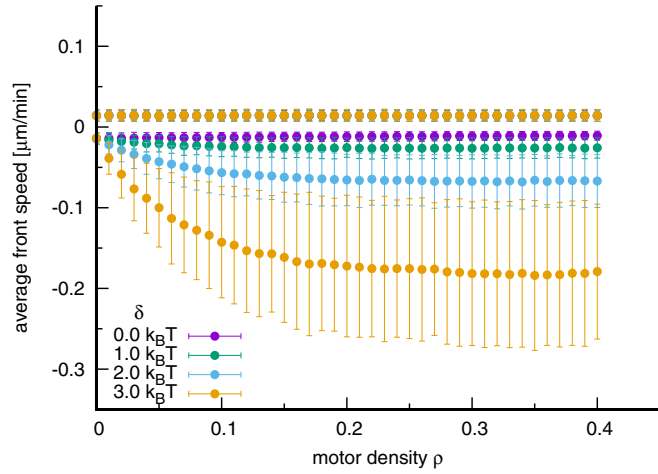
FIG. 8. Fracture process of a MT in the presence of motors. Average propagation speeds v of the damage along the MT axis for various values of the motor penalty δ as indicated in the legend. A velocity $v > 0$ ($v < 0$) indicates a propagation in the direction downstream (upstream) of the motor walking direction. The upstream propagation speed is accelerated in the presence of motors. The downstream propagation speed is independent of the presence of motors. The error bars represent the SD. Remaining parameters are $k_{\mathrm{w}} = 100\tau^{-1}$, $k_{\mathrm{r}} = 10\tau^{-1}$, $k_{-} = 1\tau^{-1}$, and as given in Table I.

tabulated ($\phi_{\mathrm{e,u}}$, $\phi_{\mathrm{g,u}}$) and ($\phi_{\mathrm{e,d}}$, $\phi_{\mathrm{g,d}}$) for the dimers immediately upstream and downstream of the defect, respectively. For simulations of MT fracture we then used the tabulated doublets of (ϕ_{e}, ϕ_{g}) to define effective off-rate constants using Eq. (5) for dimers that are nearest neighbors to vacant lattice sites using the following rules. Dimers upstream and downstream of the defect detach with the rate constants $k_{\mathrm{off,eff,u}}$ and $k_{\mathrm{off,eff,g}}$, respectively,

$$k_{\mathrm{off,eff,u}} = \left(\phi_{\mathrm{e,u}}e^{\beta\delta} + \phi_{\mathrm{g,u}}\right)k_{\mathrm{off}}^{*}e^{-\beta\Delta G_{b}}, \qquad (A4)$$

$$k_{\mathrm{off,eff,d}} = \left(\phi_{\mathrm{e,d}}e^{\beta\delta} + \phi_{\mathrm{g,d}}\right)k_{\mathrm{off}}^{*}e^{-\beta\Delta G_{b}}, \qquad (A5)$$

with $\Delta G_{b} = \Delta G_{1} + n\Delta G_{2}$ with $n = (0, 1, 2)$ determined by the lattice environment. For dimers which are lateral neighbors of the defect and experience an unperturbed motor flow the off-rate constant $k_{\mathrm{off,eff,i}}$ is given by

$$k_{\mathrm{off,eff,i}} = \left(\phi_{\mathrm{e,i}}e^{\beta\delta} + \phi_{\mathrm{g,i}}\right)k_{\mathrm{off}}^{*}e^{-\beta\Delta G_{b}} \qquad (A6)$$

with $\Delta G_{b} = 2\Delta G_{1} + \frac{n}{2}\Delta G_{2}$ with $n = (0, 1, 2, 3)$ determined by the lattice environment. Dimers which are missing one lateral and two longitudinal neighbors detach almost instantaneously from the lattice; the excitation state of the dimer is negligible for the lattice dynamics. We did not consider the detachment of dimers without a vacant neighbor site. Using full KMC simulations (simulating the motor dynamics explicitly) we checked that the distribution of dimer detachment times k_{off}^{-1} is exponential.
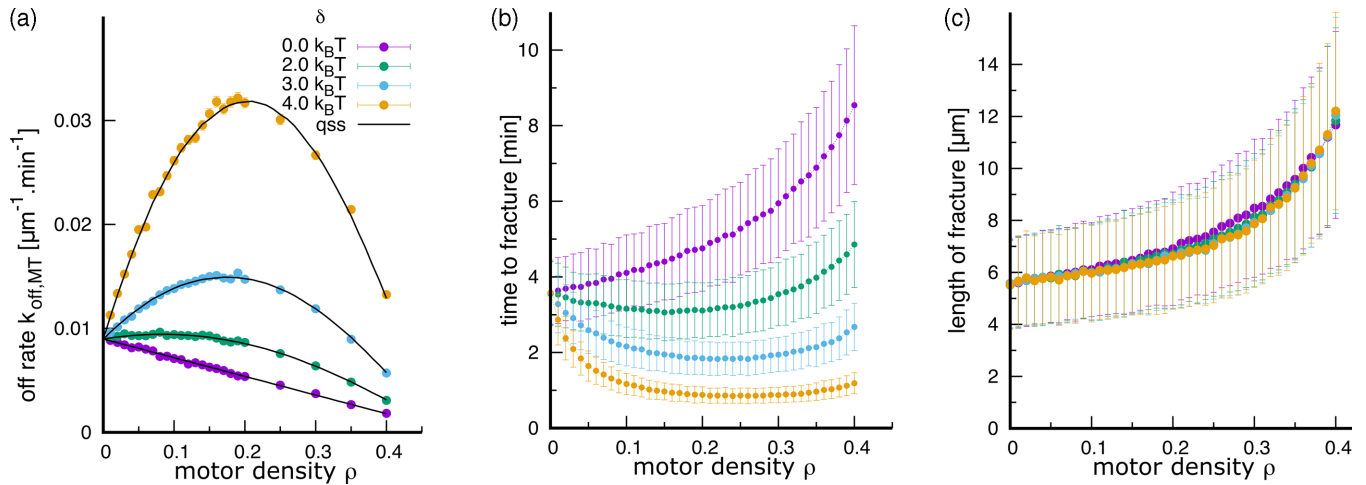

FIG. 9. Effect of slowly walking motors on the fracture of the MT shaft in the absence of free tubulin. (a) Effective rate constant for the creation of a vacancy per micrometer MT length depending on the motor density ρ for various values of the lattice excitation δ as indicated in the legend. The error bars represent the SEM. (b) Time to fracture and (c) length of damaged region at fracture after the creation of a vacancy depending on the motor density ρ for various values of the lattice excitation δ as indicated in the legend in (a). The error bars represent the SD. Remaining parameters are $k_{\mathrm{w}} = 10\tau^{-1}$, $k_{-} = 0.1\tau^{-1}$, and as given in Table I.

[1] M.-F. Carlier, Guanosine-5′-triphosphate hydrolysis and tubulin polymerization, Mol. Cell. Biochem. **47**, 97 (1982).

[2] T. Mitchison and M. W. Kirschner, Dynamic instability of microtubule growth, Nature (London) **312**, 237 (1984).

[3] R. Walker, E. T. O'Brien, N. Pryer, M. Soboeiro, W. Voter, H. Erickson, and E. D. Salmon, Dynamic instability of individual microtubules analyzed by video light microscopy: rate constants and transition frequencies, J. Cell Biol. **107**, 1437 (1988).

[4] J. Howard and A. A. Hyman, Dynamics and mechanics of the microtubule plus end, Nature (London) **422**, 753 (2003).

[5] C. Duellberg, N. I. Cade, D. Holmes, and T. Surrey, The size of the EB cap determines instantaneous microtubule stability, eLife **5**, e13470 (2016).

[6] A. Aher and A. Akhmanova, Tipping microtubule dynamics, one protofilament at a time, Curr. Opin. Cell Biol. **50**, 86 (2018).

[7] Estimates of the change in free energy upon transferring a dimer from the fully occupied lattice into the surrounding medium range from $35k_{\mathrm{B}}T$ to $80k_{\mathrm{B}}T$ per dimer [22,33,62].

[8] R. B. Dye, P. F. Flicker, D. Y. Lien, and R. C. Williams, End-stabilized microtubules observed in vitro: Stability, subunit interchange, and breakage, Cell. Mot. Cytoskel **21**, 171 (1992).

[9] A. Dimitrov, M. Quesnoit, S. Moutel, I. Cantaloube, C. Poüs, and F. Perez, Detection of GTP-tubulin conformation *in vivo* reveals a role for GTP remnants in microtubule rescues, Science **322**, 1353 (2008).

[10] T. A. Reid, C. Coombes, and M. K. Gardner, Manipulation and quantification of microtubule lattice integrity, Biol. Open **6**, 1245 (2017).

[11] L. Schaedel, S. Triclin, D. Chrétien, A. Abrieu, C. Aumeier, J. Gaillard, L. Blanchoin, M. Théry, and K. John, Lattice defects induce microtubule self-renewal, Nat. Phys. **15**, 830 (2019).

[12] L. Schaedel, K. John, J. Gaillard, M. V. Nachury, L. Blanchoin, and M. Théry, Microtubules self-repair in response to mechanical stress, Nat. Mater. **14**, 1156 (2015).

[13] A. Vemu, E. Szczesna, E. A. Zehr, J. O. Spector, N. Grigorieff, A. M. Deaconescu, and A. Roll-Mecak, Severing enzymes amplify microtubule arrays through lattice GTP-tubulin incorporation, Science **361**, eaau1504 (2018).

[14] S. Triclin, D. Inoue, J. Gaillard, Z. M. Htet, M. E. DeSantis, D. Portran, E. Derivery, C. Aumeier, L. Schaedel, K. John *et al.*, Self-repair protects microtubules from destruction by molecular motors, Nat. Mater. **20**, 883 (2021).

[15] B. G. Budaitis, S. Badieyan, Y. Yue, T. L. Blasius, D. N. Reinemann, M. J. Lang, M. A. Cianfrocco, and K. J. Verhey, A kinesin-1 variant reveals motor-induced microtubule damage in cells, Curr. Biol. **32**, P2416 (2022).

[16] Mireia Andreu-Carbó, S. Fernandes, M.-C. Velluz, K. Kruse, and C. Aumeier, Motor usage imprints microtubule stability along the shaft, Dev. Cell **57**, 5 (2022).

[17] H. de Forges, A. Pilon, I. Cantaloube, A. Pallandre, A.-M. Haghiri-Gosnet, F. Perez, and C. Poüs, Localized mechanical stress promotes microtubule rescue, Curr. Biol. **26**, 3399 (2016).

[18] C. Guyomar, S. Ku, J. Heumann, C. Bousquet, G. Guilloux, N. Gaillard, C. Heichette, L. Duchesne, M. O. Steinmetz, R. Gibeaux *et al.*, Changes in seam number and location induce holes within microtubules assembled from porcine brain tubulin and in Xenopus egg cytoplasmic extracts, Elife **11**, e83021 (2022).

[19] I. A. Schaap, P. J. De Pablo, and C. F. Schmidt, Resolving the molecular structure of microtubules under physiological conditions with scanning force microscopy, Eur. Biophys. J. **33**, 462 (2004).

[20] L. J. Davis, D. J. Odde, S. M. Block, and S. P. Gross, The importance of lattice defects in katanin-mediated microtubule severing *in vitro*, Biophys. J. **82**, 2916 (2002).

[21] Y.-W. Kuo, M. Mahamdeh, Y. Tuna, and J. Howard, The force required to remove tubulin from the microtubule lattice by pulling on its α-tubulin C-terminal tail, Nat. Commun. **13**, 3651 (2022).

[22] V. VanBuren, D. J. Odde, and L. Cassimeris, Estimates of lateral and longitudinal bond energies within the microtubule lattice, Proc. Natl. Acad. Sci. USA **99**, 6035 (2002).

[23] M. K. Gardner, B. D. Charlebois, I. M. Jánosi, J. Howard, A. J. Hunt, and D. J. Odde, Rapid microtubule self-assembly kinetics, Cell **146**, 582 (2011).

[24] Z. Wu, H.-W. Wang, W. Mu, Z. Ouyang, E. Nogales, and J. Xing, Simulations of tubulin sheet polymers as possible structural intermediates in microtubule assembly, PLoS One **4**, e7291 (2009).

[25] C. E. Coombes, A. Yamamoto, M. R. Kenzie, D. J. Odde, and M. K. Gardner, Evolving tip structures can explain age-dependent microtubule catastrophe, Curr. Biol. **23**, 1342 (2013).

[26] G. Margolin, I. V. Gregoretti, T. M. Cickovski, C. Li, W. Shi, M. S. Alber, and H. V. Goodson, The mechanisms of microtubule catastrophe and rescue: implications from analysis of a dimer-scale computational model, Mol. Biol. Cell **23**, 642 (2012).

[27] P. Pierobon, E. Frey, and T. Franosch, Driven lattice gas of dimers coupled to a bulk reservoir, Phys. Rev. E **74**, 031920 (2006).

[28] E.-M. Mandelkow, R. Schultheiss, R. Rapp, M. Müller, and E. Mandelkow, On the surface lattice of microtubules: helix starts, protofilament number, seam, and handedness, J. Cell Biol. **102**, 1067 (1986).

[29] D. Chrétien and R. H. Wade, New data on the microtubule surface lattice, Biol. Cell **71**, 161 (1991).

[30] G. M. Alushin, G. C. Lander, E. H. Kellogg, R. Zhang, D. Baker, and E. Nogales, High-resolution microtubule structures reveal the structural transitions in $\alpha\beta$-tubulin upon GTP hydrolysis, Cell **157**, 1117 (2014).

[31] M. I. Molodtsov, Elena A. Ermakova, E. A. Ermakova, E. A. Ermakova, E. E. Shnol, E. L. Grishchuk, J. R. McIntosh, and F. I. Ataullakhanov, A molecular-mechanical model of the microtubule, Biophys. J. **88**, 3167 (2005).

[32] M. Igaev and H. Grubmüller, Microtubule instability driven by longitudinal and lateral strain propagation, PLoS Comput. Biol. **16**, e1008132 (2020).

[33] D. Sept, N. A. Baker, and J. A. McCammon, The physical basis of microtubule structure and stability, Protein Sci. **12**, 2257 (2003).

[34] E. Nogales, M. Whittaker, R. A. Milligan, and K. H. Downing, High-resolution model of the microtubule, Cell **96**, 79 (1999).

[35] D. R. Peet, N. J. Burroughs, and R. A. Cross, Kinesin expands and stabilizes the GDP-microtubule lattice, Nat. Nanotechnol. **13**, 386 (2018).

[36] C. Appert-Rolland, M. Ebbinghaus, and L. Santen, Intracellular transport driven by cytoskeletal motors: General mechanisms and defects, Phys. Rep. **593**, 1 (2015).

[37] M. Rank and E. Frey, Crowding and pausing strongly affect dynamics of kinesin-1 motors along microtubules, Biophys. J. **115**, 1068 (2018).

[38] K. Visscher, M. J. Schnitzer, and S. M. Block, Single kinesin molecules studied with a molecular force clamp, Nature (London) **400**, 184 (1999).

[39] S. M. Block, Kinesin motor mechanics: Binding, stepping, tracking, gating, and limping, Biophys. J. **92**, 2986 (2007).

[40] S. L. Reck-Peterson, A. Yildiz, A. P. Carter, A. Gennerich, N. R. Zhang, and R. D. Vale, Single-molecule analysis of dynein processivity and stepping behavior, Cell **126**, 335 (2006).

[41] L. Rao, E. M. Romes, M. P. Nicholas, S. Brenner, A. Tripathy, A. Gennerich, and K. C. Slep, The yeast dynein Dyn2-Pac11 complex is a dynein dimerization/processivity factor: Structural and single-molecule characterization, Mol. Biol. Cell **24**, 2362 (2013).

[42] G. Bhabha, G. T. Johnson, C. M. Schroeder, and R. D. Vale, How dynein moves along microtubules, Trends Biochem. Sci. **41**, 94 (2016).

[43] M. W. Gramlich, L. Conway, W. H. Liang, J. A. Labastide, S. J. King, J. Xu, and J. L. Ross, Single molecule investigation of kinesin-1 motility using engineered microtubule defects, Sci. Rep. **7**, 44290 (2017).

[44] Z. Wang, S. Khan, and M. P. Sheetz, Single cytoplasmic dynein molecule movements: characterization and comparison with kinesin, Biophys. J. **69**, 2011 (1995).

[45] M. Bugiel and E. Schäffer, Three-dimensional optical tweezers tracking resolves random sideward steps of the kinesin-8 Kip3, Biophys. J. **115**, 1993 (2018).

[46] M. Bugiel, A. Mitra, S. Girardo, S. Diez, and E. Schäffer, Measuring microtubule supertwist and defects by 3D-force-clamp tracking of single kinesin-1 motors, Nano Lett. **18**, 1290 (2018).

[47] J. F. Díaz, E. Pantos, J. Bordas, and J. M. Andreu, Solution structure of GDP-tubulin double rings to 3 nm resolution and comparison with microtubules, J. Mol. Biol. **238**, 214 (1994).

[48] T. Müller-Reichert, D. Chrétien, F. Severin, and A. A. Hyman, Structural changes at microtubule ends accompanying GTP hydrolysis: information from a slowly hydrolyzable analogue of GTP, guanylyl (α, β) methylenediphosphonate, Proc. Natl. Acad. Sci. USA **95**, 3661 (1998).

[49] E. Nogales, H.-W. Wang, and H. Niederstrasser, Tubulin rings: which way do they curve? Curr. Opin. Struct. Biol. **13**, 256 (2003).

[50] S. F. Stewman, K. K. Tsui, and A. Ma, Dynamic instability from non-equilibrium structural transitions on the energy landscape of microtubule, Cell Syst. **11**, 608 (2020).

[51] J. Estévez-Gallego, F. Josa-Prado, S. Ku, R. M. Buey, F. A. Balaguer, A. E. Prota, D. Lucena-Agell, C. Kamma-Lorger, T. Yagi, H. Iwamoto *et al.*, Structural model for differential cap maturation at growing microtubule ends, eLife **9**, e50155 (2020).

[52] B. J. LaFrance, J. Roostalu, G. Henkin, B. J. Greber, R. Zhang, D. Normanno, C. O. McCollum, T. Surrey, and E. Nogales, Structural transitions in the GTP cap visualized by cryo-electron microscopy of catalytically inactive microtubules, Proc. Natl. Acad. Sci. USA **119**, e2114994119 (2022).

[53] Y. Tanaka-Takiguchi, T. J. Itoh, and H. Hotani, Visualization of the GDP-dependent switching in the growth polarity of microtubules, J. Mol. Biol. **280**, 365 (1998).

[54] O. Valiron, I. Arnal, N. Caudron, and D. Job, GDP-tubulin incorporation into growing microtubules modulates polymer stability, J. Biol. Chem. **285**, 17507 (2010).

[55] We assume that steric effects are hindering the inclusion of GTP dimers into the single vacancy of the GDP lattice, without affecting the equilibrium constant for GTP tubulin. Therefore, the detachment of GTP dimers from the GDP lattice has to be affected in the same manner as the attachment process. For GDP tubulin we assume an irreversible relaxation upon detachment from the lattice from the straight to the curved conformation, preventing any reattachment.

[56] M. Théry and L. Blanchoin, Microtubule self-repair, Curr. Opin. Cell Biol. **68**, 144 (2021).

[57] C. Aumeier, L. Schaedel, J. Gaillard, K. John, L. Blanchoin, and M. Théry, Self-repair promotes microtubule rescue, Nat. Cell Biol. **18**, 1054 (2016).

[58] J. Schaer, M. Andreu-Carbó, K. Kruse, and C. Aumeier, The effect of motor-induced shaft dynamics on microtubule stability and length, Biophys. J. **122**, 346 (2023).

[59] K. John and W. Lecompte, Data supplement for "Molecular motors enhance microtubule lattice plasticity", edited by W. Lecompte and K. John, Zenodo (2022), https://doi.org/10.5281/zenodo.7232163.

[60] J. J. Lukkien, J. P. L. Segers, P. A. J. Hilbers, R. J. Gelten, and A. P. J. Jansen, Efficient Monte Carlo methods for the simulation of catalytic surface reactions, Phys. Rev. E **58**, 2598 (1998).

[61] S. R. De Groot and P. Mazur, *Non-Equilibrium Thermodynamics* (Dover, New York, 1984).

[62] V. VanBuren, L. Cassimeris, and D. J. Odde, Mechanochemical model of microtubule structure and self-assembly kinetics, Biophys. J. **89**, 2911 (2005).

[63] A. T. Ayoub, M. Staelens, A. Prunotto, M. A. Deriu, A. Danani, M. Klobukowski, and J. A. Tuszynski, Explaining the microtubule energy balance: Contributions due to dipole moments, charges, van der Waals and solvation energy, Int. J. Mol. Sci. **18**, 2042 (2017).

[64] R. Melki, S. Fievez, and M.-F. Carlier, Continuous monitoring of P_i release following nucleotide hydrolysis in actin or tubulin assembly using 2-amino-6-mercapto-7-methylpurine ribonucleoside and purine-nucleoside phosphorylase as an enzyme-linked assay, Biochemistry **35**, 12038 (1996).

[65] J. Howard, *Mechanics of Motor Proteins and the Cytoskeleton* (Sinauer Associates, Sunderland, MA, 2001).

[66] H. P. Erickson, Co-operativity in protein-protein association: The structure and stability of the actin filament, J. Mol. Biol. **206**, 465 (1989).

[67] J. O. Andreasson, B. Milic, G.-Y. Chen, N. R. Guydosh, W. O. Hancock, and S. M. Block, Examining kinesin processivity within a general gating framework, eLife **4**, e07403 (2015).

[68] R. Jha and T. Surrey, Regulation of processive motion and microtubule localization of cytoplasmic dynein, Biochem. Soc. Trans. **43**, 48 (2015).